

## Current Source Density Reconstruction from Incomplete Data

**Daniel K. Wójcik**

*d.wojcik@nencki.gov.pl*

**Szymon Łęski**

*s.leski@nencki.gov.pl*

*Department of Neurophysiology, Nencki Institute of Experimental Biology,  
02-093 Warsaw, Poland*

We propose two ways of estimating current source density (CSD) from measurements of voltage on a Cartesian grid with missing recording points using the inverse CSD method. The simplest approach is to substitute local averages (LA) in place of missing data. A more elaborate alternative is to estimate a smaller number of CSD parameters than the actual number of recordings and to take the least-squares fit (LS). We compare the two approaches in the three-dimensional case on several sets of surrogate and experimental data, for varying numbers of missing data points, and discuss their advantages and drawbacks. One can construct CSD distributions for which one or the other approach is better. However, in general, the LA method is to be recommended as being more stable and more robust to variations in the recorded fields.

### 1 Introduction ---

A common measure of neural population activity is the local field potential (LFP), the low-frequency part of the extracellular electric potential (Nunez & Srinivasan, 2005). The LFP is generated by transmembrane currents in neighboring cells, which are usually described on a coarsely grained level by the current source density (CSD) (Plonsey, 1969; Nicholson & Freeman, 1975; Freeman & Nicholson, 1975; Mitzdorf, 1985; Nunez & Srinivasan, 2005). In the quasi-static approximation the relation of the CSD,  $C$ , to the potentials,  $\phi$ , is

$$\nabla(\sigma \nabla \phi) = -C, \quad (1.1)$$

where  $\sigma$  is the electrical conductivity tensor. For simplicity, we assume  $\sigma$  to be a constant scalar (isotropic, homogeneous medium), although in general this condition need not hold, and the assumption of a purely resistive medium may not even be valid (Holsheimer, 1987; Ibarz, Makarova, & Herreras, 2006; Logothetis, Kayser, & Oeltermann, 2007; Makarova, Gómez-Galán & Herreras, 2008). One consequence of equation 1.1 is nonlocality:

$\phi$  is not trivial even in regions where  $C = 0$ . This means that the recorded LFP may reflect the activity of quite distant cells.

When the recordings of LFP at several locations are available, one can attempt to reconstruct the CSD that generated them (Nicholson & Freeman, 1975; Freeman & Nicholson, 1975; Mitzdorf, 1985). Such recordings can be obtained, for example, with an electrode with multiple contacts or with a two-dimensional multielectrode array (Csicsvari et al., 2003; Barthó et al., 2004; Buzsáki, 2004).

The simplest method to calculate CSD is to use a numerical approximation of the second derivative of the potential (Nicholson & Freeman, 1975; Freeman & Nicholson, 1975; Mitzdorf, 1985). For example, in the case of a one-dimensional electrode with equidistant contact points spaced by  $h$ , one obtains (for interior contacts)

$$C(z_i) = -\sigma \frac{\phi(z_i + h) - 2\phi(z_i) + \phi(z_i - h)}{h^2}. \quad (1.2)$$

This approach has been extensively used to obtain and analyze CSD in a variety of experimental situations, for example, in visual (Rajkai et al., 2008), somatosensory (Lipton, Fu, Branch, & Schroeder, 2006), and auditory (Lakatos et al., 2005) cortices of macaque, in subcortical structures (Schroeder, Tenke, & Givre, 1992), in cerebellum (de Solages et al., 2008); in hippocampus (Ylinen et al., 1995); and in hippocampal slices (Shimono, Brucher, Granger, Lynch, & Taketani, 2000). However, such an approach has certain disadvantages. One of them is that equation 1.2 cannot be applied to boundary points. This is particularly inconvenient with two- or three-dimensional data, where the boundary may comprise the majority of the points (Łęski et al., 2007).

Another method for estimating the CSD is the inverse CSD (iCSD) method (Pettersen, Devor, Ulbert, Dale, & Einevoll, 2006; Łęski et al., 2007). Here one does not try to use equation 1.1 directly (which is the case in traditional CSD). Instead, the idea is to establish a one-to-one relation  $F$  between measured voltages and CSD distributions by inversion of the forward solution. This is achieved in the following way. Assume  $N$  recording points on a Cartesian grid (one-, two-, or three-dimensional). Consider an  $N$ -parameter family of CSD distributions. This means that given the values of the  $N$  parameters, one can assign a value of CSD to each spatial position. Then the values of the potential,  $\phi$ , on the grid can be obtained by solving a well-posed boundary value problem related to the elliptic partial differential equation, equation 1.1 (forward solution). Therefore, the  $N$  measured voltages are functions of the CSD parameters. If the family and the parameterization are chosen well, one can invert this relation and from the  $N$  measured potentials recover the  $N$  parameters of CSD. Usually one parameterizes the CSD with its values on the measurement grid and interpolates between the grid points, linearly or with

splines, but there are more possibilities (Pettersen et al., 2006; Łęski et al., 2007).

The aim of the inverse CSD method is to reconstruct the CSD within the volume spanned by the recording grid. Therefore, it seems natural to use in this scheme a family of CSD distributions for which the CSD is nonzero only inside the grid. However, it appears that such a choice may lead to large reconstruction errors (Łęski et al., 2007). This is because usually the actual CSD extends in the tissue beyond the grid set by the measurement points, and the sources located just outside the grid may lead to artifacts in the reconstructed density. One way to reduce these errors is to consider a family of CSD distributions extending one layer beyond the original grid. One can set the CSD values at the additional nodes to zero or duplicate the value from the neighboring node of the original grid. In Łęski et al. (2007) these two approaches were denoted by B or D boundary conditions, respectively, and it was shown that they improve the reconstruction quality within the grid. Note that the extended CSD family is still parameterized with its  $N$  values at the original grid and that the intention of such a procedure is to improve the reconstruction fidelity inside the grid and not to estimate the CSD outside.

## 2 Inverse CSD on Incomplete Data

---

A practical problem in the application of the iCSD method to real data sets is how to deal with missing recording points. Such cases arise surprisingly often in real experiments. There may be several reasons for this: a contact of a multielectrode may not be functioning, some channels may be used for other purposes (e.g., stimulation), or the experiment may be terminated early, before all the data are collected.

One way to deal with such data is to patch them with the mean of the neighboring potentials of a missing contact (Łęski et al., 2008). We denote this method by LA (local averages). This approach means replacing the missing true potential at a point with a linear approximation estimated from the neighbors. A more elaborate alternative is to reduce the size of the CSD grid and find the least-squares solution to such an overdetermined system. That means choosing such values of the parameters of the CSD spanned on a smaller grid that minimize the sum of squared differences in potential at all the available electrode points. We denote this method by LS (least squares). The advantage of this approach is that we use only the available data without making any assumptions about the missing recordings, so it seems to be better motivated than LA. However, we decrease the spatial resolution of the reconstructed CSD, so it is hard to tell a priori which approach is better.

## 3 Gaussian Sources

---

To compare the quality of the two solutions we first tested both on three-dimensional surrogate gaussian sources (see Figure 1). We calculated the

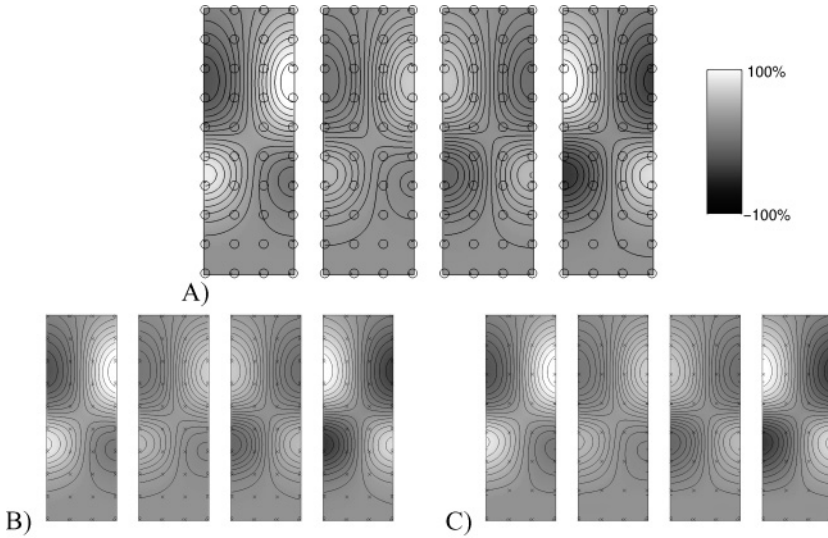


Figure 1: (A) Gaussian sources studied in section 3: four consecutive slices ( $x = 1, \dots, 4$ ) through the volume. Electrode positions are marked with circles. (B) Reconstruction of the CSD distribution spanned on the full  $4 \times 10 \times 4$  grid from the set of potentials calculated at the nodes of the grid (denoted by  $x$ 's). (C) Reconstruction using the LS method on complete data; spanned on a smaller  $4 \times 8 \times 4$  grid.

potentials on a grid of  $(x, y, z) \in 4 \times 10 \times 4$  equally spaced points. Details of the structure of the sources and calculation of LFP are given in the appendix. This choice of the sources and the grid was motivated by an experimental study of evoked potentials in the barrel cortex of the rat (J. Kamiński, private communication). The gaussian sources represent localized areas of transmembrane currents. The sources were elongated along the  $y$ -axes so that the conclusions would hold for cortical dipoles generated by active pyramidal cells. We chose this model for its simplicity, as our focus was on testing properties of the methods. The applicability of this model is limited, as it is unlikely that it would approximate the real sources in the cerebral cortex at fine spatial scales. Therefore, we do not make any statements about the actual cortical fields. For that purpose, one should use much more sophisticated models, for example, dipole generators (Tenke, Schroeder, Arezzo, & Vaughan, 1993). One could also couple cortical dynamics calculated in a neural mass model with LFP templates obtained from a detailed compartmental model of a pyramidal cell (Pettersen, Hagen, & Einevoll, 2008).

For the tests, we removed a number of virtual recording points, reconstructed the CSD using both LA and LS methods, and compared the normalized  $L^2$  reconstruction errors (Łeński et al., 2007):  $e = \int (C - \hat{C})^2 dx / \int C^2 dx$ ,

where  $C$  is the original and  $\hat{C}$  is the reconstructed CSD. For the LS method, we used a grid of  $4 \times 8 \times 4$  points that covered the whole space occupied by the original grid. This implied larger spacing in the  $y$  direction. The iCSD reconstruction was performed with the Matlab scripts from Łęski et al. (2007), modified for the situation at hand. We used not-a-knot splines with D boundary conditions.<sup>1</sup>

Standard iCSD reconstruction from the calculated potentials gives a reconstruction error  $e$  of 0.14%. This indicates the quality of the reconstructed approximation of the smooth gaussian sources by a set of splines spanned on the grid of recorded points. The LS method applied for the reduced grid gives  $e = 0.21\%$ , which shows how little information is lost when the number of nodes of the grid used for the reconstruction is reduced by 20% (see Figure 1). This is possible in this case thanks to the relatively large extent and slow variation of the sources in the  $y$  direction: the sparser grid is still dense enough to effectively sample the sources. In general, the degradation of the reconstruction quality caused by using a sparser grid will strongly depend on how rapidly the CSD varies in space (see section 4).

We have scanned all 160 cases of one recording point withdrawn. The LS method gives a stable reconstruction error from  $e = 0.21\%$  to  $e = 0.26\%$ . The error of the LA method ranges from  $e = 0.14\%$  (which means that the missing datum was indeed the mean of its neighbors) up to 2.1% (see Figure 2A).

There are 12,720 possible choices of a pair of electrodes for the set of recording points considered. Here the results are more intricate. As before, LS typically gives smaller errors (see Figure 2B), but from time to time, a huge error occurs, with  $e$  reaching 270% (63 outliers shown in an inset in Figure 2B). The outliers can occur only for specific configuration of the missing pair  $(x_1, y_1, z_1), (x_2, y_2, z_2)$ . The necessary (but not sufficient) conditions for large errors are  $(x_1, z_1) = (x_2, z_2)$  and  $(y_1, y_2) \in \{(1, 2), (1, 3), (2, 3), (9, 10), (8, 10), (8, 9)\}$ . There are only 96 such troublesome pairs, and all of the outliers in Figure 2B are of this type.

With a growing number of missing recording points, the reconstructions become less and less reliable, with the LS method becoming monotonically worse with respect to the LA method (see Figures 2C and 2D). Interestingly, the distributions of the results qualitatively have the same character as in the case of two missing electrodes: that is, the errors of LA method have a unimodal distribution, while the distributions of errors in the LS approach have two modes— one with results better than for LA and the other with extremely large errors. The mean error of the LA method also grows, but

---

<sup>1</sup>By D boundary conditions, we mean solution on a larger grid with one extra layer added in every direction beyond the original. We assume identical CSD at the added layer and its nearest neighbor in the original grid. “Not-a-knot” splines are the cubic splines implemented in Matlab. They differ from “normal” splines in the conditions at the extreme points. See Łęski et al. (2007) for details.

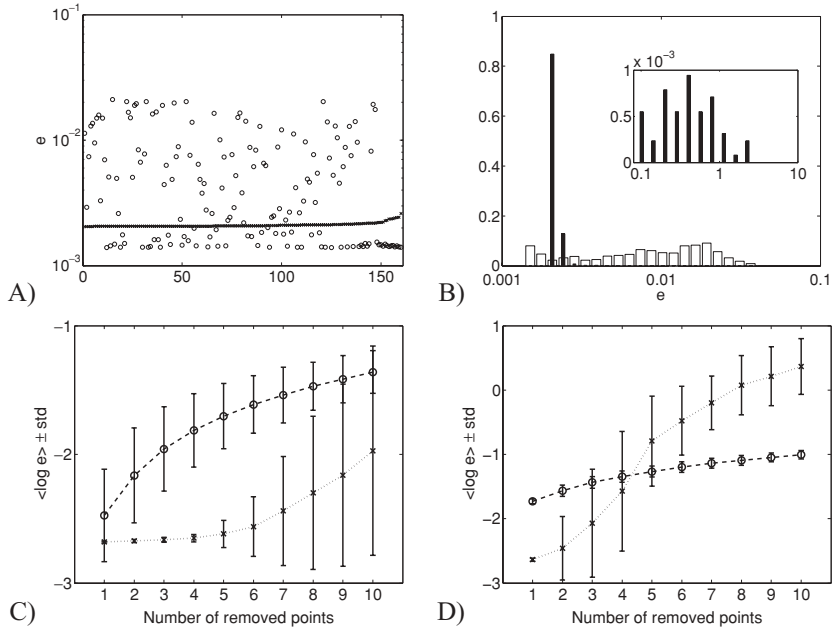


Figure 2: Comparison of local averages (LA) and least squares (LS) methods of reconstructing CSD from incomplete data. (A) Results of reconstruction in the case of a single recording point removed from the grid. Normalized reconstruction error for all 160 possibilities, LS: x's; LA: o's, sorted according to the LS error. (B) Histogram of normalized reconstruction errors for a pair of grid points removed. Thick bars: LA; thin bars: LS. Inset: outliers in the LS method. (C) Comparison of LA (o's) and LS (x's) methods for varying number  $n$  of recording points removed from the grid (x-axis). y-axis: average logarithm of normalized reconstruction error. Error bars are  $\pm$  standard deviation, for the best 90% out of 2000 random choices of removed points (except  $n = 1$  where 90% of all 160 possibilities are taken). (D) Same as C but for the worst 10% of the cases.

huge errors do not occur. Figures 2C and 2D show the results obtained for 2000 random choices of the missing recording points.

#### 4 Experimental Data

The second part of the test of the two methods was performed on three-dimensional recordings in the rat forebrain of potentials evoked by the deflection of a bunch of whiskers (Łęski et al., 2007). The recordings were made on a grid of  $4 \times 5 \times 7$  points. Here we analyze the same two representative latencies used as illustrations in Łęski et al. (2007), where the data set is described in detail.

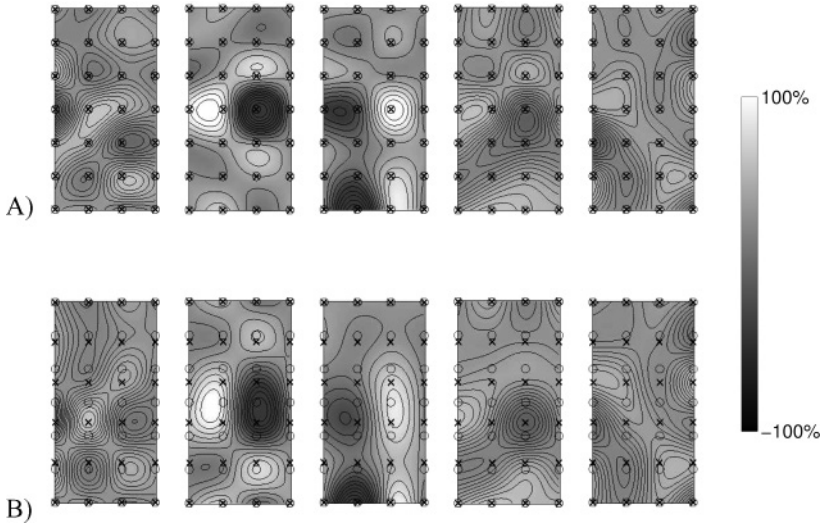


Figure 3: Reconstructions of CSD from experimental data,  $t = 3.5$  ms, after stimulation of the vibrissa. Each row presents a three-dimensional region of the rat forebrain. The electrode positions ( $4 \times 5 \times 7$  grid) are marked with circles, and the nodes of the grid are marked with x's. (A) Reference data set: CSD reconstructed on the full electrode grid. (B) CSD reconstructed from the complete set of recordings but spanned on a sparser  $4 \times 5 \times 6$  grid. Note that some sources are not adequately sampled using the sparser grid.

We perform the same analysis as for the gaussian sources, apart from the fact that now we do not know the real CSD. Therefore, as the reference  $C$ , we take the reconstruction spanned on the full  $4 \times 5 \times 7$  grid calculated from the full set of recordings. Such  $C$  is the best representation of real CSD in the tissue available to us.

Figure 3A shows the reference data set, and Figure 3B shows the CSD reconstructed by the LS method on a sparser  $4 \times 5 \times 6$  grid from the complete set of recorded potentials, 3.5 ms after the stimulus onset. Already we can observe how the intricate structure of activation in the tissue is distorted ( $e = 21\%$ ) when using a smaller spanning grid, which was not the case for the gaussian sources modeling the cortical CSD (see section 3).

Clearly, in performing reconstructions from incomplete data, we expect the distortions to grow. Results of the test of the two methods are shown in Figure 4. Figure 4A shows the results of the iCSD reconstructions from data with one electrode removed. As in the previous case, the distribution of errors of the LS method is bimodal with very narrow modes, while the distribution of errors of the LA method is rather broad (see Figure 4B). However, unlike the previous case, the LA method is almost always better.

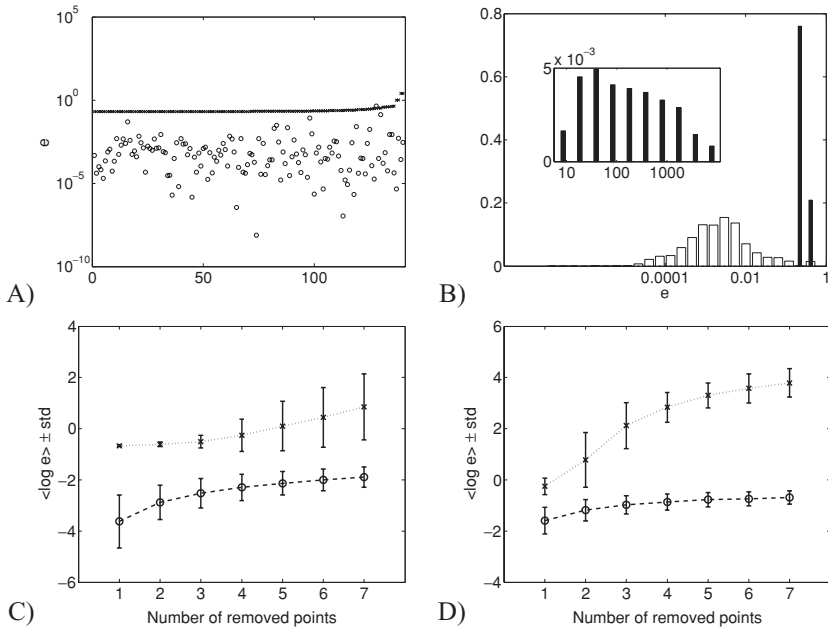


Figure 4: Comparison of LA and LS methods of reconstructing CSD from incomplete data; see the Figure 2 caption. The data used here are the same as in Figure 3.

This difference is preserved as the number of removed points is increased. For both methods, the mean error of reconstruction grows with the number of removed points, which is expected. However, the distribution of errors for the LS methods gets wider, while the distribution of errors for LA method gets narrower. This is true for both the best 90% of cases and the 10% worst. In practice, this means that the LS method for such complicated CSD distributions is not recommended.

Such behavior was typical for this data set for the time frames we inspected. For illustration and comparison, we show the reconstructions from the complete data on the original (see Figure 5A) and smaller (see Figure 5B) grids, as well as the results of the same analysis for the recordings taken 15 ms after the stimulus onset (see Figure 6).

## 5 Discussion

Reconstruction of the current source density generating recorded extracellular potentials from these potentials is an ill-defined problem. The reason is that there is an infinite number of different distributions, which could

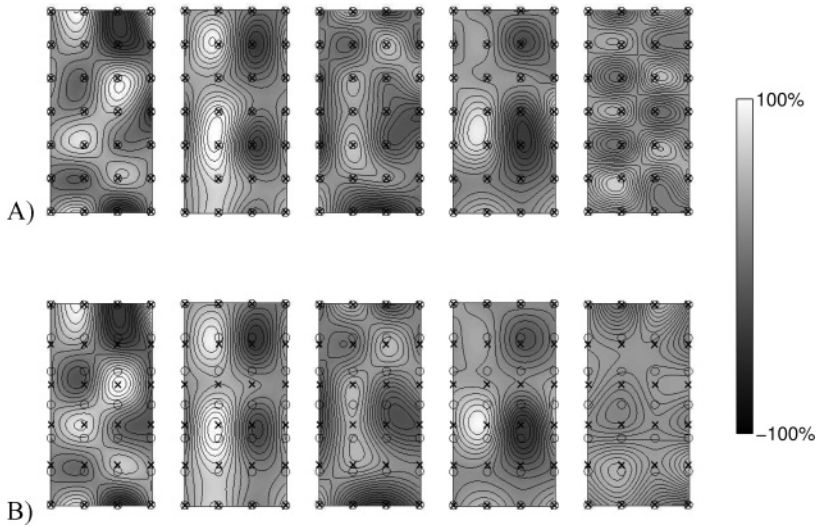


Figure 5: Reconstructions of CSD from experimental data,  $t = 15$  ms, after stimulation of the vibrissa. For description, see the Figure 3 caption.

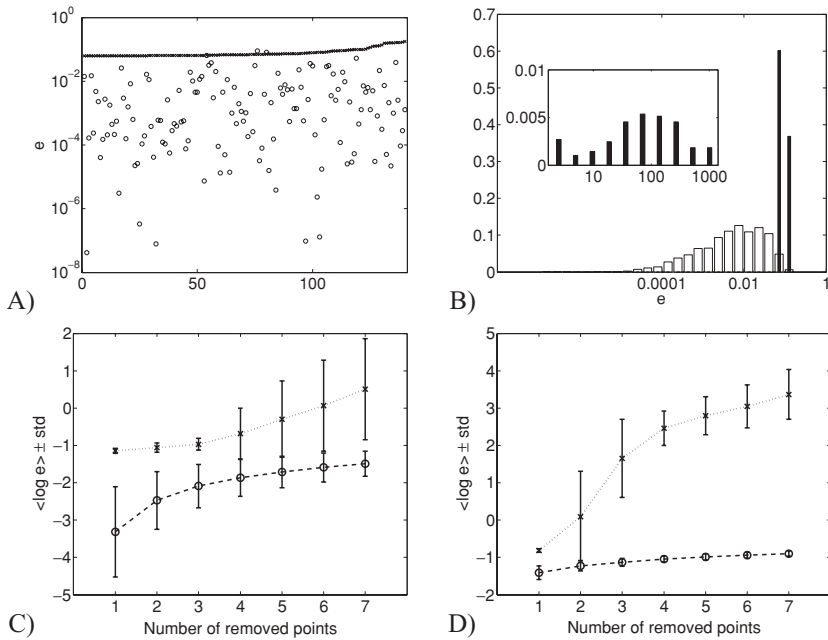


Figure 6: Comparison of LA and LS methods of reconstructing CSD from incomplete data; see the Figure 2 caption. The data used here are the same as in Figure 5.

lead to the same recordings. Nevertheless, as the CSD is much more a local reflection of the neural activity than the potentials, there were many attempts to find a viable reconstruction of the sources from the measured fields (Nicholson & Freeman, 1975; Mitzdorf, 1985; Pettersen et al., 2006). One recent candidate, which has a number of advantages over the classical approach, is the inverse CSD method (Pettersen et al., 2006; Łęski et al., 2007). It was originally developed for situations where a set of recordings was collected on a regular rectangular grid. Given the construction of the method, it is unclear how to proceed when one of the recordings is missing due to a failure of one of the electrode contacts or in other cases. We have discussed here two approaches that might enable the application of iCSD method to sets with incomplete data.

The LA method is simple and stable, and the results are never very bad (normalized error of the order of a few percent), even for a relatively large number of missing data points. The LS method seems attractive, as it does not assume anything about the missing data. The distribution of errors is usually bimodal with two narrow modes. Usually the errors are within a small range dominated by the effect of the sparser grid; however, for a subset of cases growing with the number of missing data, the errors can be extremely large.

The respective quality of reconstruction for the two methods depends on the structure of the original sources and (especially for LS) the specific location of the removed points. Our tests on the sources modeling the dipole distributions of the cortex (see section 3) with the grid shrinking along the dipole show that for a small number of missing recording points (fewer than five), the LS method usually gives smaller errors than the LA. However, for more complex thalamic sources (see section 4), the LA method is usually far better for any number of removed points.

A priori, it is not obvious which method to choose in analysis of experimental data, when the original CSD is unknown and is to be found. Our recommendation is to use the LA method in all cases. Despite its simplicity, it seems to be more stable and leads to smaller errors, especially for complex distributions; thus, it becomes our method of choice. If the potential seems to vary relatively slowly along one direction of the grid and the missing data are not nearest neighbors lying at the edge, the LS method might also be worth trying, but in general we do not recommend it.

One may wonder if it is possible to improve the technique beyond the proposed approaches. One way would be to consider CSD distributions spanned on the available recording points, which would not necessarily form a full regular grid. However, this seems rather difficult to implement in full generality, as the spline coefficients would have to be calculated from scratch for every distribution of the recording points, and the matrix connecting the potentials with the CSD parameters would have to be calculated for every distribution, adding substantially to the computational overhead. A more promising approach seems to be the application of statistical

Table 1: Coefficients of the Gaussian Sources.

$i$	1	2	3	4	5	6	7	8
$x_i$	1	4	1	4	1	4	1	4
$y_i$	1	1	4	4	1	1	4	4
$z_i$	3.5	3.5	3.5	3.5	6.5	6.5	6.5	6.5
$\sigma_i^{xz}$	1	1	1	1	1	1	1	1
$\sigma_i^y$	1.5	1.5	1.5	1.5	1	1	1	1
$A_i$	0.8	-1.1	-1.2	1	-1	1.2	0.5	-0.9

Note: Origin of the grid is  $(x, y, z) = (1, 1, 1)$ .

methods. For example, in the future, we plan to use an overdetermined basis of gaussian sources and search for efficient projections of the recordings on this basis.

## Appendix: Gaussian Test Sources

The gaussian sources used in the test in section 3 were of the form

$$C(x, y, z) = \sum_{i=1}^8 A_i \exp \left[ -\frac{(x - x_i)^2}{2(\sigma_i^{xz})^2} - \frac{(y - y_i)^2}{2(\sigma_i^y)^2} - \frac{(z - z_i)^2}{2(\sigma_i^{xz})^2} \right],$$

with the coefficients given in Table 1. Figure 1 shows four parallel sections of the sources, which together pass through all the nodes of the grid (in the region spanned by the virtual recording grid). To calculate the potentials, we truncated the sources to the region  $-1 \leq x \leq 6$ ,  $-1 \leq y \leq 12$ ,  $-1 \leq z \leq 6$ .

## Acknowledgments

This work was partly financed by the Polish Ministry of Science and Higher Education research grants N401 146 31/3239 and PBZ/MNiSW/07/2006/11. S.Ł. was supported by the Foundation for Polish Science.

## References

- Barthó, P., Hirase, H., Monconduit, L., Zugaro, M., Harris, K. D., & Buzsáki, G. (2004). Characterization of neocortical principal cells and interneurons by network interactions and extracellular features. *J. Neurophysiol.*, 92(1), 600–608.
- Buzsáki, G. (2004). Large-scale recording of neuronal ensembles. *Nat. Neurosci.*, 7(5), 446–451.
- Csicsvari, J., Henze, D. A., Jamieson, B., Harris, K. D., Sirota, A., Barthó, P., et al. (2003). Massively parallel recording of unit and local field potentials with silicon-based electrodes. *J. Neurophysiol.*, 90(2), 1314–1323.

- de Solages, C., Szapiro, G., Brunel, N., Hakim, V., Isope, P., Buisseret, P., et al. (2008). High-frequency organization and synchrony of activity in the Purkinje cell layer of the cerebellum. *Neuron*, 58(5), 775–788.
- Freeman, J. A., & Nicholson, C. (1975). Experimental optimization of current source-density technique for anuran cerebellum. *J. Neurophysiol.*, 38(2), 369–382.
- Holsheimer, J. (1987). Electrical conductivity of the hippocampal CA1 layers and application to current-source-density analysis. *Exp. Brain. Res.*, 67(2), 402–410.
- Ibarz, J. M., Makarova, I., & Herreras, O. (2006). Relation of apical dendritic spikes to output decision in CA1 pyramidal cells during synchronous activation: A computational study. *Eur. J. Neurosci.*, 23(5), 1219–1233.
- Lakatos, P., Shah, A. S., Knuth, K. H., Ulbert, I., Karmos, G., & Schroeder, C. E. (2005). An oscillatory hierarchy controlling neuronal excitability and stimulus processing in the auditory cortex. *J. Neurophysiol.*, 94(3), 1904–1911.
- Łęski, S., Wójcik, D. K., Tereszczuk, J., Świąjkowski, D. A., Kublik, E., & Wróbel, A. (2007). Inverse current-source density method in 3D: Reconstruction fidelity, boundary effects, and influence of distant sources. *Neuroinformatics*, 5(4), 207–222.
- Łęski, S., Pettersen, K. H., Einevoll, G. T., Gigg, J., Kublik, E., Świąjkowski, D. A., et al. (2008). *The inverse current source density (iCSD) method: Precise estimation of CSD from multielectrode recordings with one, two and three dimensional contact grids*. Presentation at the Society for Neuroscience Annual Meeting, Washington, DC.
- Lipton, M. L., Fu, K.-M. G., Branch, C. A., & Schroeder, C. E. (2006). Ipsilateral hand input to area 3b revealed by converging hemodynamic and electrophysiological analyses in macaque monkeys. *J. Neurosci.*, 26(1), 180–185.
- Logothetis, N. K., Kayser, C., & Oeltermann, P. A. (2007). In vivo measurement of cortical impedance spectrum in monkeys: Implications for signal propagation. *Neuron*, 55(5), 809–823.
- Makarova, J., Gómez-Galán, M., & Herreras, O. (2008). Variations in tissue resistivity and in the extension of activated neuron domains shape the voltage signal during spreading depression in the CA1 in vivo. *Eur. J. Neurosci.*, 27(2), 444–456.
- Mitzdorf, U. (1985). Current source-density method and application in cat cerebral cortex: Investigation of evoked potentials and EEG phenomena. *Physiol. Rev.*, 65(1), 37–100.
- Nicholson, C., & Freeman, J. A. (1975). Theory of current source-density analysis and determination of conductivity tensor for anuran cerebellum. *J. Neurophysiol.*, 38(2), 356–368.
- Nunez, P. L., & Srinivasan, R. (2005). *Electric fields of the brain: The neurophysics of EEG*. New York: Oxford University Press.
- Pettersen, K. H., Devor, A., Ulbert, I., Dale, A. M., & Einevoll, G. T. (2006). Current-source density estimation based on inversion of electrostatic forward solution: Effects of finite extent of neuronal activity and conductivity discontinuities. *J. Neurosci. Methods*, 154(1–2), 116–133.
- Pettersen, K. H., Hagen, E., & Einevoll, G. T. (2008). Estimation of population firing rates and current source densities from laminar electrode recordings. *J. Comput. Neurosci.*, 24(3), 291–313.
- Plonsey, R. (1969). *Bioelectric phenomena*. New York: McGraw-Hill.

- Rajkai, C., Lakatos, P., Chen, C.-M., Pincze, Z., Karmos, G., & Schroeder, C. E. (2008). Transient cortical excitation at the onset of visual fixation. *Cereb. Cortex*, *18*(1), 200–209.
- Schroeder, C. E., Tenke, C. E., & Givre, S. J. (1992). Subcortical contributions to the surface-recorded flash-VEP in the awake macaque. *Electroencephalogr. Clin. Neurophysiol.*, *84*(3), 219–231.
- Shimono, K., Brucher, F., Granger, R., Lynch, G., & Taketani, M. (2000). Origins and distribution of cholinergically induced beta rhythms in hippocampal slices. *J. Neurosci.*, *20*(22), 8462–8473.
- Tenke, C. E., Schroeder, C. E., Arezzo, J. C., & Vaughan Jr., H. G. (1993). Interpretation of high-resolution current source density profiles: A simulation of sublaminar contributions to the visual evoked potential. *Exp. Brain. Res.*, *94*(2), 183–192.
- Ylinen, A., Bragin, A., Nádasdy, Z., Jand, G., Szabó, I., Sik, A., et al. (1995). Sharp wave-associated high-frequency oscillation (200 Hz) in the intact hippocampus: Network and intracellular mechanisms. *J. Neurosci.*, *15*(1 Pt 1), 30–46.

---

Received July 31, 2008; accepted April 30, 2009.